CHAPTER 5. IMPROVEMENT IN THE BALLISTIC PERFORMANCE

5.1 Approach methodology

The results of the first series of ballistic tests and the recommendations formulated in Chapter 4 constitute the basis for the ballistic improvement in steels E and H and the development of the chemical compositions for the further eight advanced performance armour steels P through to W and their appropriate heat treatment. The thickness range of the plates to be tested was reduced from 6 mm to between 4.5 and 5.2 mm in order to introduce a further safety factor in the maximum protection of the cockpit and the passenger cell with 6 mm thick armour plate. The volume fraction of the retained austenite in the plate martensite is considered to be the main factor determining the ratio of the yield strength to ultimate tensile strength (YS/UTS) of the armour steels and their resistance to localised yielding and perforation during a ballistic impact.

The morphology of the martensite and the volume fraction of the retained austenite after water quenching of the steels are *inter alia* functions of the martensite start temperature, which in turn, is a function of the chemical composition and the austenitising conditions. The latter effect provides effective dissolution of the carbides into the austenite matrix, which modifies its chemical composition and thus its chemical driving force for the martensitic transformation. Moreover the grain size of the parent austenite that grows with increasing austenitisation temperature and time, determines the total volume of the grain boundaries where the heterogeneous nucleation of the martensite can initiate. Consequently, the following reverse procedure was adopted in determining the chemical composition of the further eight advanced performance armour steels:

- The retained austenite (RA) located in the plate inter-faces was more effective in reducing the ratio YS/UTS than the RA located in the lath inter-faces. The optimum range of the volume fraction of retained austenite for an advanced ballistic performance was estimated at between 2% to 7%;

- The martensite start temperature of the advanced armour steels should, therefore, be lower then 210°C to enhance the formation of plate martensite over lath martensite;

- Using the proposed formula in Equation (4.14), the chemical compositions within the range specified in Section 4.4.2.3 to obtain eight suitable compositions, was found with predicted martensite start temperatures ranging from 100°C to 200°C within a ±30°C error. The chemical compositions of the eight steels P through to W were thus determined through this procedure;

- The steels were produced in a vacuum melting furnace, Calcium treated and degassed and cast into 5 kg ingots before being solution treated at 1050°C for one hour, hot rolled to thicknesses of 4.5 ± 0.2 or to 5.2 ± 0.2 mm, directly quenched into water at room temperature and lastly tempered at 180°C or at 250°C for 20 minutes;

- Samples for thin foil transmission electron microscopy before the ballistic testing and those for the determination of the martensite start temperature, were cut from these plates;

- The ballistic testing was performed and samples are cut from the impact regions for the X-ray diffraction analysis of the retained austenite, for the scanning electron microscopy of the cracks and for the thin foil transmission electron microscopy. The micro-hardness profiles across the impact region were also determined;

- Differences between the microstructures before and after the ballistic impact are explained;

- A revised specification, comprising the chemical composition range, the heat treatment and the mechanical properties for the high performance 6 mm steel armour plates is then formulated.

The chemical compositions of the steels P through to W, as determined by the above procedure, are given in Table (4.3.32). The martensite start temperatures after austenitisation determined by dilatometric analysis and those calculated, are included in Table (5.1). The volume fraction of the retained austenite before the ballistic test, determined by X-ray diffraction is also included in the same table.

Table (5.1): Martensite start temperatures and volume fraction of retained austenite in the tempered steels P through to W before ballistic testing

	Martensite start temperatures °C		**Volume fraction of retained austenite**	**Vickers hardness**
Designation of the armour steel	**Measured**	**Calculated using the formula (4.27)**	**%**	**VHN (30kg)**
P	115	63	6	580
Q	178	63	4	615
R	170	141	3	610
S	182	141	3	510
T	184	172	0.6	578
U	170	164	2	510
V	145	150	5.3	595
W	130	140	6	565

The volume fraction of retained austenite was determined within a 0.5% standard deviation.

5.2. Ballistic report

Plates of these eight armour steels were tested in the same ballistic conditions than those of the earlier steels E, F, G and H. The results of this second series of ballistic testing are reported in Table (5.2).

The steel T was the only that did not pass the ballistic test despite its higher hardness and thickness. Typical photographs of the front and of the rear faces of the plates that passed the test well from this second series of ballistic testing are shown in Figure 5.1.

Table (5.2): Ballistic report of the steels P through to W

Plate	Plate thickness	Firing distance (Meter)	Firing angle (°)	Hardness (VHN)	Projectile Velocity (m/s)	Ballistic performance
					933	Passed well
					928	Passed well
Steel P	4.7	30	0	580	931	Passed well
					955	Passed well
					952	Passed well
					947	Passed well
					943	Passed well
Steel Q	4.9	30	0	615	937	Passed well
					948	Passed well
					938	Passed well
					947	Passed well
					939	Passed well
Steel R	5.1	30	0	610	946	Passed well
					935	Passed well
					947	Passed well
					942	Passed well
					940	Passed well
Steel S	5.2	30	0	578	947	Passed well
					942	Passed well
					952	Passed well
					944	Failed Clean Penetration
					945	Failed Clean Penetration
Steel T	5.4	30	0	610	945	Failed Clean Penetration
					945	Failed Clean Penetration
					935	Failed Clean Penetration
					941	Failed Clean Penetration
					939	Passed well
					941	Passed well
Steel U	4.9	30	0	578	951	Passed well
					951	Passed well
					961	Passed well
					938	Passed well
					947	Passed well
Steel V	5.1	30	0	595	947	Passed well
					948	Passed well
					952	Passed well
					952	Passed well

Table 5.2 Continued						
					942	Passed well
					935	Passed well
Steel W	4.8	30	0	565	941	Passed well
					941	Passed well
					931	Passed well

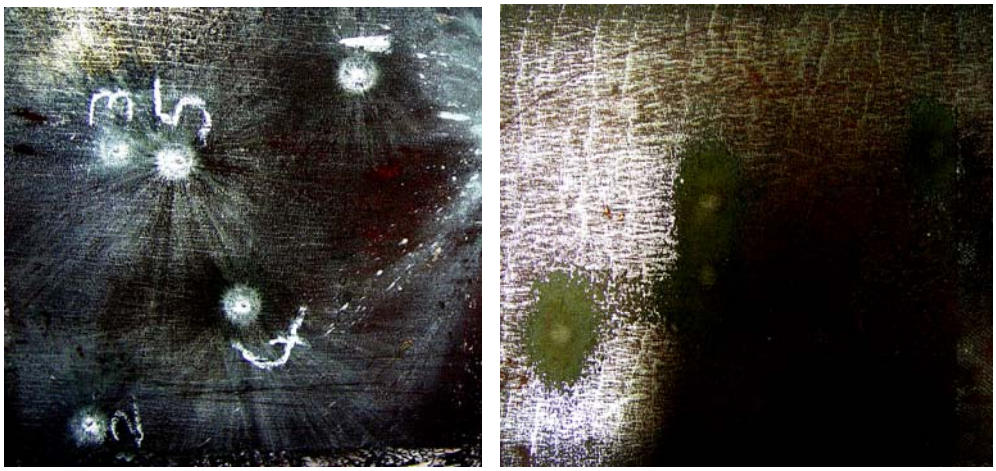

(a) Image of the front face of steel Q plate **(b)** Image of the rear face of steel Q plate

Figure 5.1: Photographs of the impact regions of the 4.9 mm steel Q plate that passed the ballistic testing

It is concluded from Table (5.2) that only steel T, containing the lowest volume fraction of retained austenite of about 0.6% did not pass the ballistic test.

5.3 The Ballistic Parameters

Visual observation of the areas affected by the ballistic impact revealed three concentric domains around the incidence point of the fired round in the armour plate. These three domains may also be observed around the penetration hole in plate T that failed the test. The size of these domains indicates the resistance to localised yielding of the armour plate. The existence of these three domains in the perforated plate of steel T that failed the ballistic test, may be explained by the relatively high velocity of the "slower" plastic wave that follows the precursor "faster" elastic wave compared to the longitudinal movement of the fired round through the thickness of the plate.

The inner domain, zone 1, that may be seen from the rear face in Figure 5.1(b), is penetrated more into the plate and had almost the same diameter in all eight plates, irrespective of whether the plate passed or failed the test. The thickness of the plates and the volume fraction of retained austenite in these steels seemed to have very little effect on the diameter of this inner zone 1. The diameter of the intermediate domain, zone 2, on the other hand differed while the diameter of the outer domain, zone 3, differed significantly.

The zones 2 and 3 are distinguishable on the front face as shown in Figure 5.1(a). The diameters of these three circular domains within the ballistic impact-affected areas are given in Table (5.3) for these eight steels.

Table (5.3): Diameters of the three concentric zones within the ballistic impact affected areas of the armour plates tested

	Thickness of the plate [mm]	Volume fraction of retained austenite [%]	Diameter zone 1 [mm]	Diameter zone 2 [mm]	Diameter zone 3 [mm]	Ballistic parameter BP
Steel P	4.7	6	13	26	54	0.0546
Steel Q	4.9	4	12	24	46	0.0298
Steel R	5.1	2	13	28	48	0.0061
Steel S	5.2	3	12	27	44	0.0165
Steel T	5.4	0.6	7	8	24	0.0027
Steel U	5.1	2	13	28	40	0.0061
Steel V	5.1	5.3	13	26	50	0.0323
Steel W	4.8	6	12	30	56	0.0494

The differences between these diameters as well as their variations are shown by plotting their values versus a ballistic parameter, defined as follows:

$$\mathrm{BP} = \frac{\mathrm{RA}(\%)}{\mathrm{EXP}(\delta)} \qquad (5.1)$$

where RA is the volume fraction of retained austenite and δ is the thickness of the steel plate in millimeters. The choice of this expression for the BP parameter is based, firstly on the proportional lowering of the ratio of YS/UTS by the retained austenite and secondly, on the increase of the effective penetrating weight when the thickness of the plate increases because of the direct transmission of the linear momentum to the cylinder of material ahead of the fired round within the plate. Figure 5.2 is a graphic presentation of the diameters of the three zones as functions of the ballistic parameter BP.

More ballistic testing is necessary before determining an accurate mathematical description of the diameters of the three zones in terms of the ballistic parameter BP. Nevertheless, the general shape of the curves in Figure 5.2 may suggest that within the range of the experimental parameters used, including the impact velocity, the firing angle, the volume fraction of the retained austenite and the thickness for the martensitic steel armour plates, the optimum ballistic performance is realised for values of the ballistic parameter BP between 0.0180 and 0.060.

The ballistic performance may decrease again at higher values of the parameter, whose limit is yet to be determined experimentally, because of a too high volume fraction of retained austenite or because of a too low thickness of the steel plate. The minimum hardness and the minimum thickness requirement of the armour steels should then be determined and the feasible region for the ballistic application redefined.

The ballistic parameter BP of the steels P through to W calculated as defined by Equation (5.1) are shown in Table (5.3). Plotting the measured diameters of the three concentric zones 1, 2 and 3 also shown in Table (5.3), produces the following Figure 5.2.

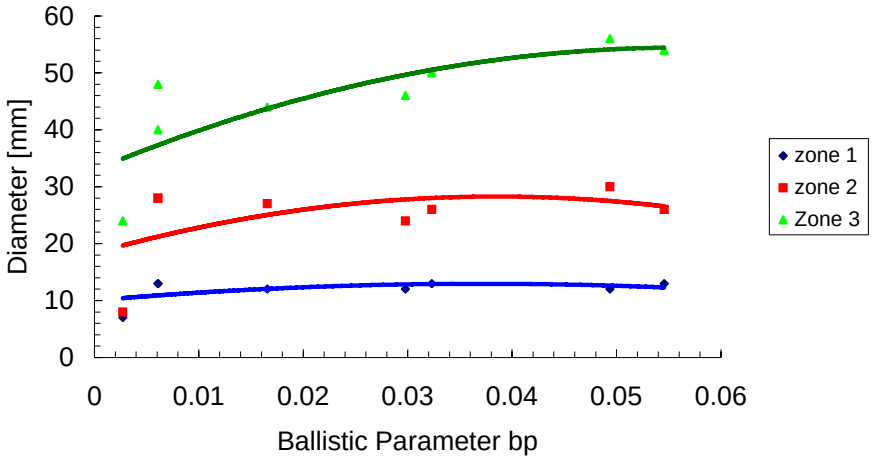

Figure 5.2: Variation of the diameters of the concentric zones 1, 2 and 3 within the ballistic impact affected domains as functions of the BP parameter.

The material in zone 1 is heated up to high temperatures during the impact as suggested by the scanning electron microscopy of the surface of the armour plates that are covered by the molten lead from the fired rounds. The temperature and pressure within these zones was high enough to cause welding of the copper and the lead from the fired round to the steel plates. The effect of the temperature rise on the microstructure within these zones was examined through thin foil electron microscopy after the ballistic testing by cutting specific localised 3 mm discs from these zones with a spark erosion wire cutting machine.

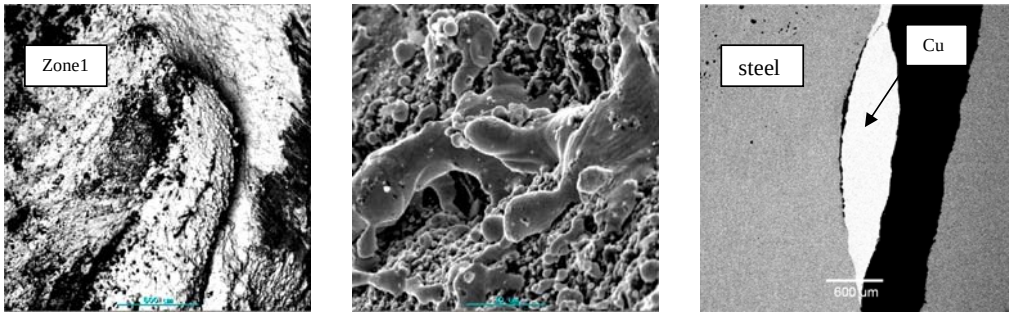

5.3(a) **5.3(b)** **5.3(c)**

Figure 5.3: Secondary electron scanning electron microscopy of zone 1's front face of steel plate R covered with molten lead form the fired round (Figures 5.3 (a) and 5.3(b), label mark: 500µm). A polished cross section of zone 1 showing the copper from the fired round welded to the plates (figure 5.3(c)).

Figure 5.3(a) also illustrates the wavelike separation of the material within zone 1 by being dragged into the plate thickness. This illustrates the known theory, which predicts that at high strain rates and high temperatures the solid steel behaves like a dynamic liquid. Scanning electron microscopy of the cross-section of some impact regions revealed the presence of a tri-dimensional crack, the so-called Hopkinson sphere [5], formed where the compressive elastic

wave was reflected from the outer edges of the plate. This composed an additional interference wave together with the slow compressive plastic wave, which produced a tensile stress higher than the true fracture stress of the armour steel. Closer observation of the crack demonstrates that the crack was composed of micro-cracks propagating along the grain boundaries outwards from the impact sphere. Figure 5.4 shows a typical cross section cut from one of the plates after ballistic testing.

Figure 5.4: Cross section throughout the affected impact region showing the copper from the round attached on to the front face of a 4.8 mm steel W plate. The bending of the plate in the affected impact region is also observable.

Figure 5.5 shows the tri–dimensional crack and the dynamic micro-cracks along the grain boundaries within the cross-section of the impact region. The surfaces in Figures 5.5(a) and 5.5(b) were not etched whereas the one in Figure 5.5(c) was etched.

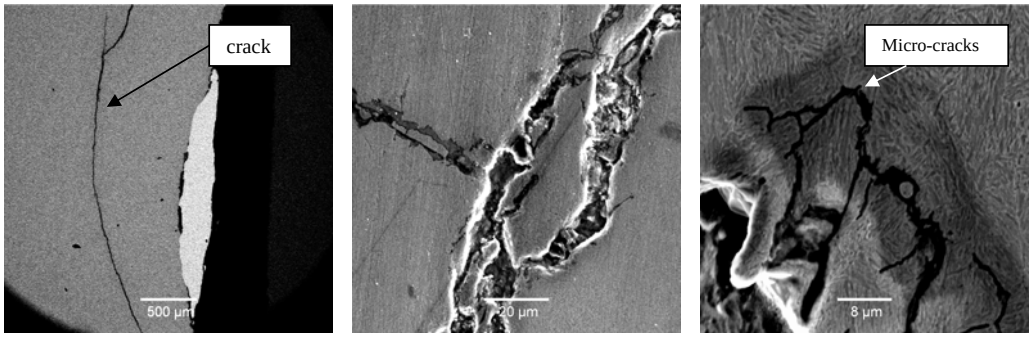

5.5(a) 5.5(b) 5.5(c)

Figure 5.5: Backscatter scanning electron microscopy of the Hopkinson sphere and the micro-cracks formed dynamically within the tensile region

The micro-cracks along the grain boundaries demonstrate the significance of the grain boundary properties on its ballistic performance of an armour steel. Clean grain boundaries without segregated particles or precipitates will have a higher cohesion strength and, therefore, a better resistance against the pull-out of grains due to the high tensile stress that occurs near to the spherical crack. The micro-crack substructures were encountered within the cross sections of steel R that passed the ballistic test and also in the plate of steel T that failed the ballistic test. These two steels were similar in their lower volume fraction of retained austenite. This observation may confirm that the retained austenite also arrests the propagation of the micro-cracks initiated in the region where high tensile stress waves are formed during the ballistic impact. The literature reports levels of tensile stress as high as 28 GPa [16, 17, 18] that may develop in the steel armour plate during the ballistic impact before fracture.

The untempered armour steels U and V also complied with the requirement of the specifications for ballistic performance but they also had macro-cracks and some parts were

actually broken-off from the plate. The broken sections were about fifteen centimetres from the centre of the impact region as shown in Figure 5.6.

Figure 5.6: Untempered armour plate of steel U fractured by impact loading during ballistic testing showing the fracture some centimetres away from the impact points.

This observation agrees with the theory of an additional shock wave interference at a certain distance from the impact point, formed between a precursor "faster" compressive elastic wave reflected as a tensile wave by the edges of the plate and a following "slower" compressive plastic wave. The distance at which interference between the two waves will take place and reach such an amplitude that the true fracture strength of the material at high strain rate is exceeded, depends on the mass and velocity of the fired round as well as the mass, Young's modulus and the density of the plate.

The relation between stress wave propagation and fracture has been studied for more than a hundred years. B Hopkinson [quoted in 5], in his published paper on " The Effects of Momentary Stresses in Metals" where he repeated his father's work, provided an explanation of the rather puzzling phenomenon of spalling or scabbing. It is characteristic of the impact of high-speed projectiles or the detonation of explosive charges in contact with brittle targets. In this phenomenon, which takes place when an impact occurs on one side of a brittle plate, most of the fractures are observed not near the point of impact, but at the opposite free surface of the plate away from the impact region. J. Hopkinson [quoted in 5] in his paper on " On the Rupture of Iron Wire by blow" had showed that the following surprising results occurred:

- "The effects of two blows, which will break the wire, were not equal when the momentum or the energies were equal, but when the velocity of the mass at impact reached a certain critical value";
- In his experimental conditions the wire did not break near to the point at which the impact took place but fractured further away.

In this Section the explanation that J. Hopkinson gave in the case of the drop weight impact test, was adapted to the case of a ballistic impact on a steel plate as follows:

1. The tensile stress σ_0 associated with a particle velocity $\overline{V}_0$ is $\rho\overline{V}_0 c_0$, where ρ is the density of the wire. c_0 is the velocity of extension waves in the wire;
2. $c_0 = (E/\rho)^{1/2}$ where E is Young's modulus;
3. The maximum particle velocity $\overline{V}_0$ is equal to the velocity of the fired round and plate system immediately after impact;
4. Then, if the impact is inelastic, $\overline{V}_0 = [2ghM/(M+m)]^{1/2}$, where M is the mass of the fired round and m is the mass of the plate;
5. The falling height h is converted in to the round's velocity V as follows: $h \approx V^2/2g$.
6. Then $\overline{V}_0 = [V^2 M/(M+m)]^{1/2}$;
7. The tensile stress associated with the velocity $\overline{V}_0$ is $\sigma_0 = \rho c_0 V[M/(M+m)]^{1/2}$;
8. The peak stress in the pulse is dependent on V, M and m. The tensile stress after superposition between the reflected pulse and the incident one is $2\sigma_0 = 2\rho c_0 V[M/(M+m)]^{1/2}$;
9. If the tensile strength of the plate is σ, the condition for fracture near the clamping support of the plate is $\sigma = 2\sigma_0$

$$V_F = \frac{\sigma}{2\rho c_0 [M/(M+m)]^{1/2}} \qquad (5.2)$$

where V_f is the minimum velocity of the round at which fracture will occur. The condition for fracture to occur near the top of the plate is $\sigma = \sigma_0$ or:

$$V_F = \frac{\sigma}{\rho c_0 [M/(M+m)]^{1/2}} \qquad (5.3)$$

Taylor [5] has pointed out that the situation is in fact much more complicated than J. Hopkinson had realized, since the pulse produced by the impact has an infinitely long "tail".

The model considered by Taylor can be adapted to the case of ballistic impact as follows:

1. The equation of motion of the fired round and the plate after impact is $M\,dV/dt = A\sigma = A\rho V c_0$, where A is the cross sectional area of the plate and V is the velocity of plate and round at time t. The solution of this equation is:

$$V = \overline{V}_0 \exp[-\rho A c_0 t / M] \qquad (5.4)$$

where $\overline{V}_0$ is the combined velocity at time t=0;
2. Thus, the stress at the clamp holding the plate is given by $\sigma = \rho c_0 V = \rho c_0 \overline{V}_0 \exp(-\rho A c_0 t/M)$ and a sharp-fronted pulse with an exponential decay travels through the plate;

3. The stress at a distance x from the clamp is given by:

$$\sigma(x,t) = \rho c_0 \bar{V}_0 \exp[\rho A/M(x - c_0 t)] \qquad (5.5)$$

4. Equation (5.5) can also be written as:

$$\sigma(x,t) = \rho c_0 \bar{V}_0 \exp[\beta(x - c_0 t)] \qquad (5.5(a))$$

5. These conditions apply for times up to $t = L/c_0$, where L is the distance between the impact point and the point where the wave front reaches the clamping support and the pulse is reflected. Since the plate support is fixed the reflected pulse is one of tension and in the time region $L/c_0 < t < 2L/c_0$ for $0 < x < (2L - c_0 t)$, one has only the tail of the incident pulse, i.e. $\sigma(x,t) = \rho c_0 \bar{V}_0 \exp[\beta(x - c_0 t)]$;
6. For $x > (2L - c_0 t)$, one has the superposition of the reflected tensile pulse and the tail of the incident pulse, i.e.:

$$\sigma = \rho c_0 \bar{V}_0 \{\exp \beta[(2L - x) - c_0 t] + \exp \beta(x - c_0 t)\}. \qquad (5.6)$$

7. Now, the reflected pulse will once again be reflected at the plate support but since the mass is finite, this reflection will result in a change in the velocity of the plate and the round's mass M and after this reflection, there will be three superimposed waves in the plate;
8. The process will continue and can result in stresses greater than the stress of $2\rho \bar{V}_0 c_0$ postulated by J. Hopkinson. The degree to which this value is exceeded depends on a nondimensional parameter α, which is the ratio $M/(L\rho A)$, i.e. the ratio of the mass of the fired round to the mass of the plate. Taylor has shown that this maximum stress is given approximately by the expression:

$$\bar{\sigma} = \rho c_0 \bar{V}_0 \left[1 + \alpha^{-1/2}\right] \qquad (5.7)$$

Thus Taylor predicts $\bar{\sigma} = 4.2 \rho c_0 \bar{V}_0$ rather than $\bar{\sigma} = 2 \rho c_0 \bar{V}_0$ as postulated by J. Hopkinson and this occurs later than at the third reflection at the plate support. Hammond and Proud [16] recently reported stress values as high as 28 GPa, or a multiplying factor of 12 instead of 4.2 as in the above relation of the maximum tensile stress being reached during a ballistic impact in a 12 mm thick steel plate. The common idea in all of these estimates is that the steel can resist higher tensile stresses dynamically than statically, a conclusion that is supported by the usual strain rate dependence of the flow stress of most metals.

It is possible to design an armoured structure in such a manner that the transmissibility between the plates and the structure-support is higher to allow a controlled fraction of the incident energy to flow into the structure, thereby reducing the amount of energy reflected into the plate. But this solution should be carefully examined in order not to destroy the integrity of the support-structure and its reliability. Another solution may be the lengthening of the transmissibility path such that the elastic as well as the plastic waves are attenuated in such a

way that their interference does not induce stresses higher than the true fracture stress of the armour steel during ballistic impact.

The stress distribution within the plate as a function of the time and the distance from the plate-support is presented in Figure 5.7. For this calculation the average mass of the plates is estimated at 4.5kg, the density of the steel is 7800kg/m^3, the mass of the round is 3.5g and the striking velocity is 940m/s. The results of the calculation are presented in Table (5.4).

Table (5.4): Predicted theoretical characteristics of the plate – round system during the ballistic impact, using the model proposed by Taylor [5].

Characteristics				
Velocity of the pressure wave front c_0 [m/s]	**Velocity of the system plate-round V_0 [m/s]**	**Predicted yield strength σ_0 [MPa]**	**Spalling strength S_0 [MPa]**	**Dynamic tensile strength σ_{max} [GPa]**
5063	27.1	1071	1070	38

This model predicts the uniaxial tensile strength to be at about 1071 MPa and the true fracture stress due to dynamic impact loading, at about 38 GPa for these armour steels. The difference between the measured maximum stress reported by Hammond and Proud [16] and others [17, 18] with the predicted value of 38 GPa, may be explained by the neglect of the influence of any existing defects present in the material in the theoretical model. Any such defects will reduce the effective dynamic fracture strength of the steel armour plates according to the well-known principles of elastic fracture mechanics. The analysis of Equation (5.6) shows that the stress distribution throughout the plate is strongly dependent on the time of stress wave travel. The stress distribution in the region between one and two hundred centimetres wave path length from the centre of impact is shown in Figure 5.7. The model predicts a tensile stress of between 11.7 GPa and 13.2 GPa in that region in which the fracture lines are located. This means that the fracture occurs between the fourth and the fifth reflections of the tensile wave from the edges of the plate.

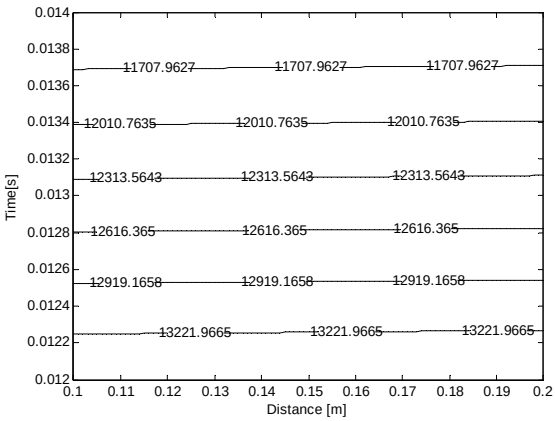

Figure 5.7: Predicted tensile stress distribution within the plates tested in this study due to the ballistic impact, as a function of the time and wave path length measured from the impact point and considering reflection at the top end on Figure 5.6.

5.3. The fracture mechanism due to the high strain rate during ballistic testing of plates of steels P through to W

The shear lips of the fractured surfaces of the untempered steels U and V plates were analysed by secondary electron scanning to identify the mechanism of the crack initiation and its propagation. Two directions of propagation of the cracks were observed throughout the fractured sections. The first three–dimensional crack propagated in a cylindrical surface whose generator lies parallel to the surface of the plate. The second crack propagated in a direction transverse to the surface of the plate and this crack determined the fractured surface. Figure 5.8 shows these three-dimensional cracks near the edges of the untempered steel U plates.

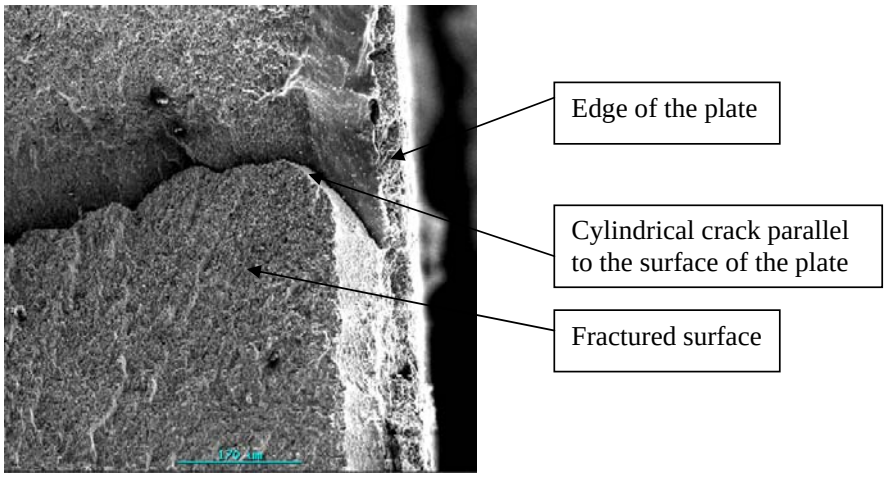

Figure 5.8: Secondary electron scanning microscopy of the shear lips of the fractured surface near the edge of the untempered plate of steel U. Label mark 170μm.

The scanning electron microscopy also revealed shear bands that cross the fractured surfaces of the untempered plates. These bands suggest that the ballistic impact induces cyclic loading in the plates due to the multiple reflections of the tensile stress wave from the edges of the plates. The shapes of the shear bands indicate that the fracture further away from the impact region, initiates near the edge of the plate and propagates cyclically throughout the thickness resulting in complete fracture. Such shear bands are shown in Figure 5.9. The initiation of these cracks near the edge of the plate verifies the earlier proposal of a reflection of the compressive wave as a high stress tensile wave from the edges as proposed by Taylor. The cracks were probably initiated just after the first or the second reflection of the tensile wave from the edge because of the poor mechanical behaviour of the untempered martensite under tensile stress in these plates.

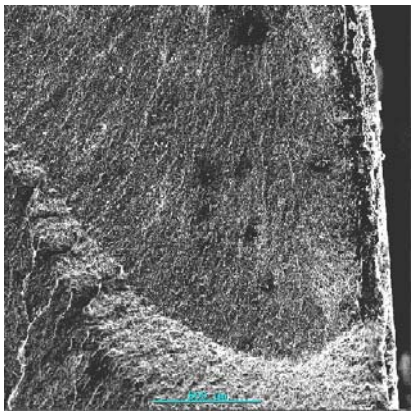

Figure 5.9: Secondary electron scanning microscopy showing the shear bands in the fractured surface of the untempered steel U plate at 12cm far from the impact point. Label mark 500μm.

The shear bands have two different appearances depending on the distance from the initiation point. Near the edge of the plate the shear lips of the broken plate are smooth with very fine dimples as shown in Figure 5.10(a), while a brittle inter-granular fracture of Figure 5.10(b), with blocks of grains being pulled out was observed at about one millimetre depth into the plate, as shown in Figure 5.10(c).

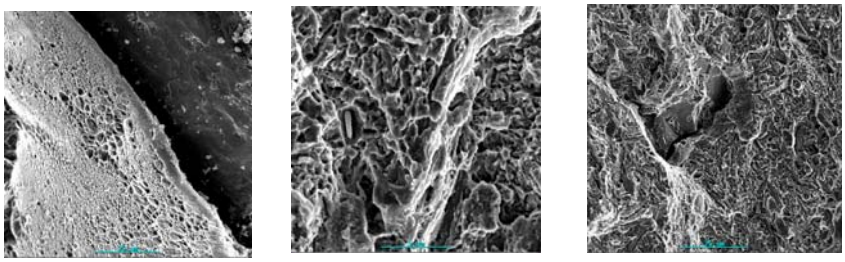

(a) (b) (c)

Figure 5.10: Secondary electron scanning microscopy of the shear lips showing two different modes of fracture in the same fractured surface (a) smooth shear lips with fine dimples observed near the edges of the fractured surface. (b) and (c) brittle fracture away from the edges where unstable propagation of the crack took place. Label mark 2.8μm.

From Figures 5.10(b) and (c) it appears that the grain boundaries may be a low resistance path for the propagation of the tensile stress wave caused by the ballistic impact through the entire thickness of the armour plate.

The ballistic impact excites the natural vibration modes of the plates. The first natural frequency of the armour plate should then be kept higher than the highest excitation frequency of the firing rifle to avoid any synchronisation that will lead to a catastrophic spalling of the plates. The mass, stiffness, damping factors and shape are the main parameters that determine the natural resonant frequencies of the plates. The mass and the length of the plate can easily be controlled and reduced through design so that the first natural frequency is high. The reduction of the mass is possible by manufacturing thinner and smaller plates, as was the entire aim of this study.

The stiffness and the damping factors of the plate depend on the microstructure that is inherited from the chemical composition and the heat treatment applied to the armour plate.
Considering that the microstructure is optimised for the ballistic performance, only the mass and the shape of the plates may practically be changed to take into account the effect of the excitation frequency of the firing rifle.

5.4. Morphology of the martensite and microstructures of the steels P through to W that were tested ballistically

The microstructures of the above mentioned armour steels were analysed before and after the ballistic test to identify any differences between them for the purpose of finding a direct relationship between the microstructure and its ballistic performance. The effect of the strength of the armour plate on the perforation of the plates using different projectile nose shapes has been investigated recently by Dey and Borvik [15]. They found that when a blunt projectile hits the target, the material in front of the projectile accelerates, while the rest of the target is relatively stationary. Hence, the deformation localises in narrow shear bands under adiabatic conditions where the shear strain, shear strain rate and temperature may locally be very high. According to their study [15], these shear bands may either consist of only *deformed* material or *transformed* material depending on the temperature that was reached in this localised area.

Mescheryakov and Divakov [17] have concluded from their investigation into the shock-induced structural transitions and dynamic strength of solids, following from the analysis of peculiarities of high-velocity penetration and also from the analysis of experimental data, that the strength-component of the resistance of solids to penetration (as a complementary factor to the inertial forces) is determined by the resistance to plastic deformation. This means that if the character of the plastic deformation changes, for example, because of a change in the structural mechanism of deformation, the strength-component of the resistance to penetration changes as well. Recent studies based on the measurement of the mechanical properties of armour steels, confirm the need for the understanding of the ballistic performance of these armour plates based on their microstructural behaviour. Hammond and Proud [16], in their work on the pressure-induced ($\alpha - \varepsilon$) phase transformation in low-alloy steels, where they have measured and compared the ballistic performance of lower and upper bainite respectively in terms of the Hugoniot Elastic Limits and spalling strength of these two phases, have concluded:

" In order to understand why the materials behaved as they did and possibly to predict material properties in the future, it is important to investigate the microstructural response to the different impact conditions. This could take the form of microscopy, X-ray diffraction and hardness testing. Such research may help to establish why the phase transition was not observed in upper bainite and why the Hugoniot Elastic Limits of the two materials are so different".

They have found the HELs to be 3.5 ± 0.5 GPa and 2 ± 0.5 GPa for the lower and higher bainite respectively. The lower-bainite was found to have a phase transition at 13 ± 0.5 GPa.

The eight plates from Table (5.3) were sectioned after the ballistic tests for different analyses and micro-hardness measurements. X-ray diffraction analysis was done in the cross section of the impact-affected zones (Figure 5.4) to determine the volume fraction of the retained austenite after the ballistic impact.

Table (5.5): Volume fraction of the austenite in the impact-affected regions before and after ballistic testing

	Thickness of the plate [mm]	Volume fraction of retained austenite before testing [%]	Volume fraction of retained austenite after ballistic testing [%]
Steel P	4.7	6	<0.5
Steel Q	4.9	4	<0.5
Steel R	5.1	2	<0.5
Steel S	5.2	3	<0.5
Steel T	5.4	0.6	<0.5
Steel U	5.1	2	<0.5
Steel V	5.1	5.3	<0.5
Steel W	4.8	6	<0.5

The volume fraction of the retained austenite in the impact-affected regions are systematically lower after the ballistic testing than before, indicating a transformation process.

The Vickers micro-hardness profiles of the same cross-sections of steels P, Q R, T and W were compared to appreciate the significance of the work hardening of the armour steel plate in resisting ballistic perforation. The plates of the steels P, Q, R, T and W were selected on the basis of their initial volume fraction of retained austenite, their plate thickness and the ballistic behaviour. The comparison was then possible firstly, between the armour plates that all had passed the ballistic test and secondly, between those that passed the tests and the plate of steel T that had failed the test. Three lines of measurement were drawn on each cross section of the impact-affected zones. The first line was drawn at one mm depth from the incidence surface and the second one at 2.5 mm and the third one at 4.5 mm depth. The Vickers micro-hardness was measured along each line with the reference zero point for the measurement along a line intersecting the line and the incidence direction of the fired round which is also the longitudinal axis of the deformed volume, shown by the arrow in the figure below.

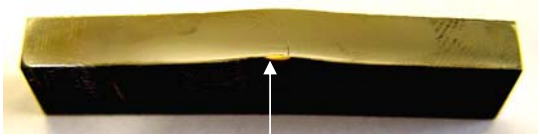

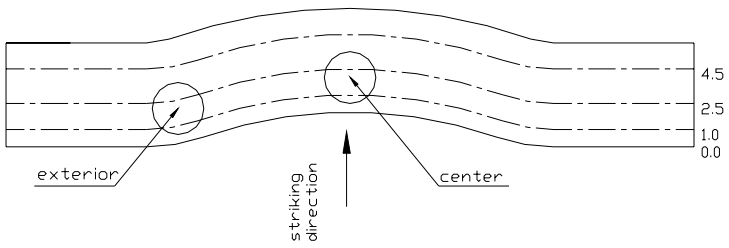

Figure 5.11: Illustration of the principle for the drawing of the iso-depth lines along which the micro-hardness was measured and the positions from where 3mm discs were cut for thin foil TEM. The arrow shows the incidence direction of the fired round.

The measured Vickers micro-hardnesses are given in Table 5.6:

Table (5.6): Vickers micro-hardness throughout the cross section of the deformed zones after the ballistic testing

	Vickers micro-hardness											
Depth from the impacted surface	**Distance from the incidence direction of the fired round[mm]**											
Steel P (4.7mm)	**1**	**2**	**3**	**5**	**7.5**	**10**	**12.5**	**15**	**17.5**	**20**	**25**	
1 mm	639	648	671	671	680	622	622	639	622	622	606	
2.5 mm	594	626	666	652	685	639	626	639	620	606	594	
4.5 mm	710	710	746	705	639	644	644	644	626	622	598	
Steel Q (4.9mm)	**1**	**2**	**3**	**5**	**7.5**	**10**	**12.5**	**15**	**17.5**	**20**	**25**	
1 mm	551	564	568	575	575	579	537	537	537	537	537	
2.5 mm	564	550	564	598	554	543	537	537	530	530	530	
4.5 mm	602	602	602	602	602	561	564	537	530	530	530	
Steel R (5.1mm)	**1**	**2**	**3**	**5**	**7.5**	**10**	**12.5**	**15**	**17.5**	**20**	**25**	
1 mm	496	575	583	590	583	579	571	598	588	583	598	
2.5 mm	626	652	661	631	648	639	598	594	618	598	598	
4.5 mm	661	635	635	690	652	639	639	610	602	586	598	
Steel W (4.8mm))	**1**	**2**	**3**	**5**	**7.5**	**10**	**12.5**	**15**	**17.5**	**20**	**25**	**30**
1 mm	657	666	671	666	657	671	661	666	639	644	614	622
2.5 mm	661	622	648	657	666	648	648	648	648	639	639	626
4.5 mm	661	685	675	675	675	635	630	631	606	614	614	614
Steel T (5.4mm)				**5**	**7.5**	**10**	**12.5**	**15**	**17.5**	**20**	**25**	
1 mm				614	505	481	446	427	422	422	422	
2.5 mm				602	564	523	523	517	517	515	511	
4.5 mm				511	514	499	505	508	505	508	508	

The hardness measurements start at approximately 6 millimetres from the axis of the perforation hole for the plate of the steel T that failed the test. These hardnesses are compared in Figure 5.12.

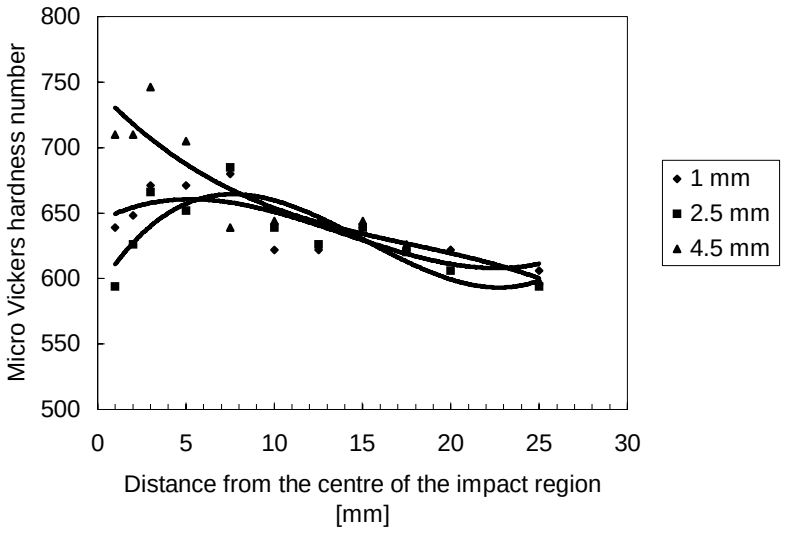

Figure 5.12(a): Vickers micro-hardness profiles throughout the cross section of the deformed zone of the plate of steel P

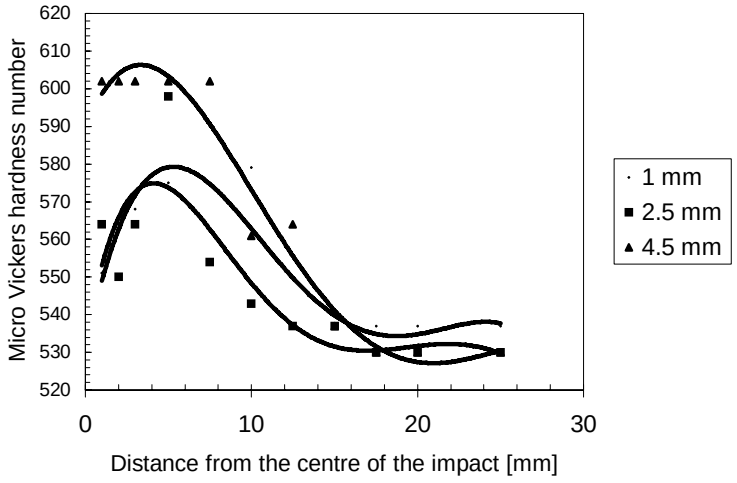

Figure 5.12(b): Vickers micro-hardness profiles throughout the cross section of the deformed zone of the plate of steel Q

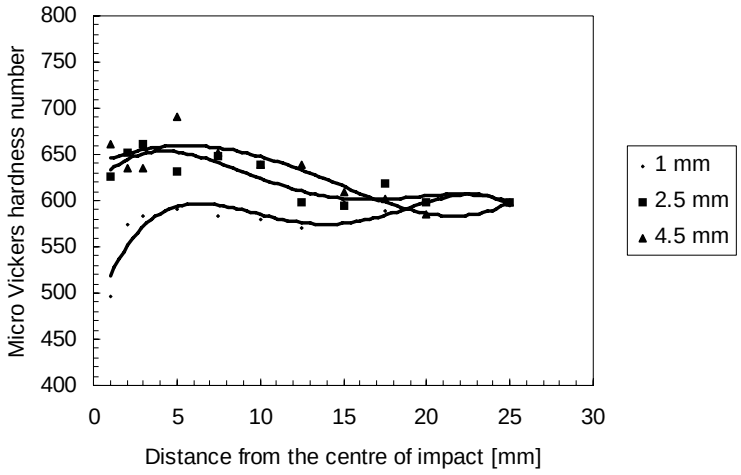

Figure 5.12(c): Vickers micro-hardness profiles throughout the cross section of the deformed zone of the plate of steel R

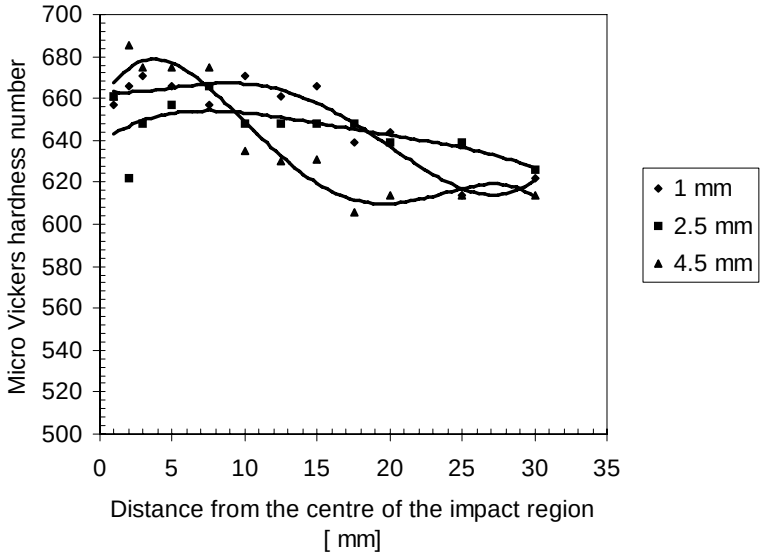

Figure 5.12 (d): Vickers micro-hardness profiles throughout the cross section of the deformed zone of the plate of steel W

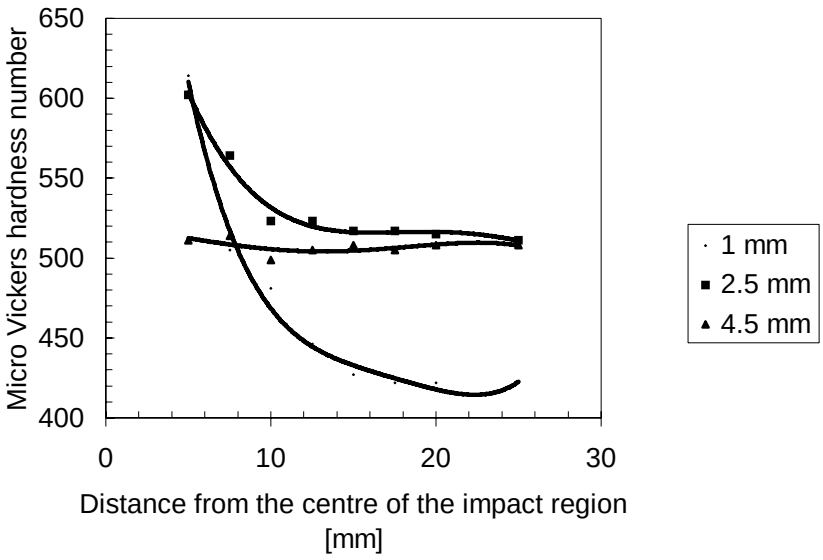

Figure 5.12(e): Vickers micro-hardness profiles throughout the cross section of the deformed zone of the plate of steel T that had failed the test

The following observations can be made:

(i) For the plates that withstood the fired round, the hardnesses near the incidence direction, i.e. in zone 1, are higher for the iso-depth lines situated at 4.5 mm from the incidence surface than for the iso-depth lines situated at 1 and 2.5 mm . For the latter two iso-depth lines the hardness curves have a maximum at about 10 mm from the incidence direction of the fired round while the hardnesses within zone 1 are lower. The Vickers micro-hardness on the iso-depth-lines at 4.5 mm increased by about 100 units for the steels P, Q and W that had a higher volume fraction of retained austenite before the ballistic testing than steel R with only 2% retained austenite and whose hardness increased only by about 50 units.

(ii) The plate of steel R with 2% retained austenite, showed a decrease in hardness along the 1 mm iso-depth line compared to the hardness at 25 mm further away from the impact incidence direction. This is opposite to the tendency in the plates of steels P, Q and W with higher volume fractions of retained austenite.

(iii) The plate of steel T that had failed the test had a higher hardness around the perforation hole for the iso-depth lines at 1 and 2.5 mm and a lower hardness for the iso-depth line at 4.5 mm. This is again opposite to the observation in the non-perforated plates of steels P, Q, R and W. Moreover steel T had softened during the ballistic impact.

Thin foils cut by spark erosion from the same zones were analysed in transmission electron microscopy to examine the differences between these steels and the variation in their hardnesses in the cross section of the same steel.
Three areas were selected on each cross section for the cutting of the thin foils, i.e. the centre of the impacted region (center in Figure 5.11), the circumference of the deformed zone

(exterior in Figure 5.11) and the non-deformed area. The bright field and dark field images of these areas are compared below:

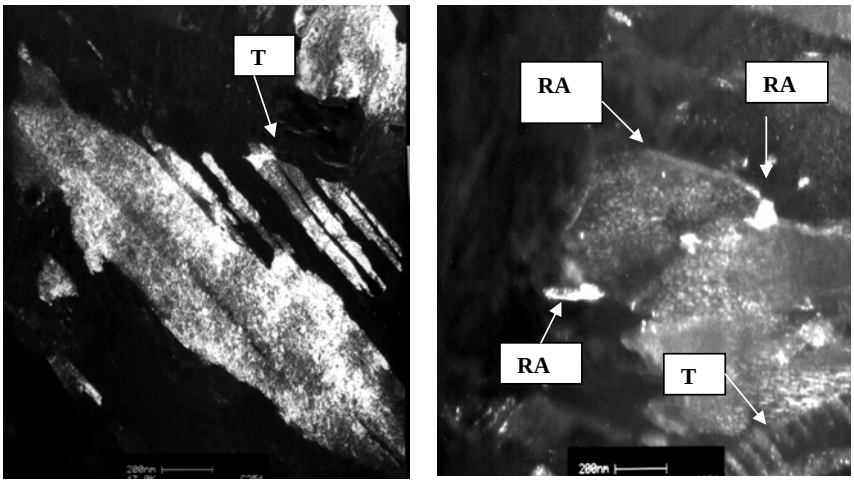

(a) **(b)**

Figure 5.13: Dark field transmission electron microscopy showing the twinned martensite with retained austenite in steel P before the ballistic test.

Two types of shape of the retained austenite were observed in the dark field image in Figure 5.13(b), i.e. a nodular type and an interplate film type along the plate interfaces.

The microstructure of steel Q was close to that of steel P, consisting of twinned martensite with retained austenite along the plate interfaces.

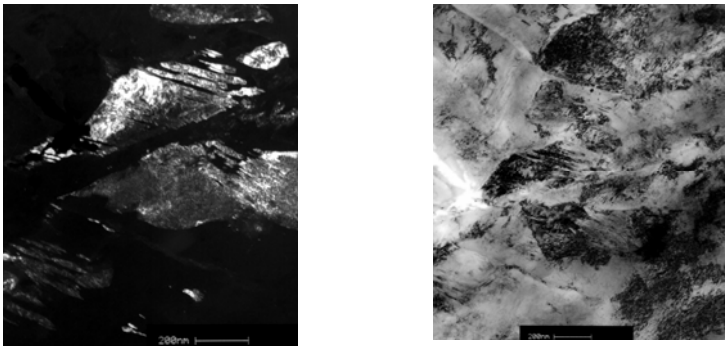

(a) (b)

Figure 5.14: Transmission electron microscopy of steel Q, (a) dark field image and (b) corresponding bright field image of the twinned martensite.

The thin foil images of transmission electron microscopy from the centre of the impact and from the circumference of the deformed region are compared below. At the centre of the impact "new" martensite was formed. Fine carbides were precipitated within the martensite matrix and no twins were observable.

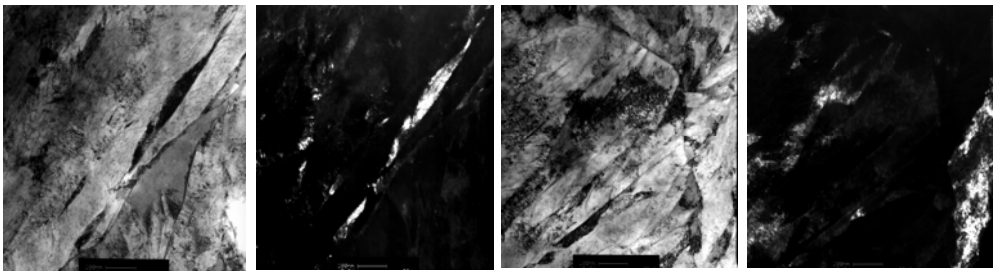

(a) **(b)** **(c)** **(d)**

Figure 5.15: Transmission electron microscopy of the centre of impact of steel Q; (a) and (c) bright field images, (b) and (e) respective corresponding dark field images showing no twins and neither retained austenite after ballistic test. Label mark 200 nm.

The absence of twinned martensite in the "new martensite" could arise from incomplete solution of carbide, diluting the austenite and raising the Ms temperature.
Because reaustenitisation occurs transiently in the impact zone the properties of austenite will be important in energy absorption and ballistic resistance. The kinetics of reaustenitisation will also be composition dependent.

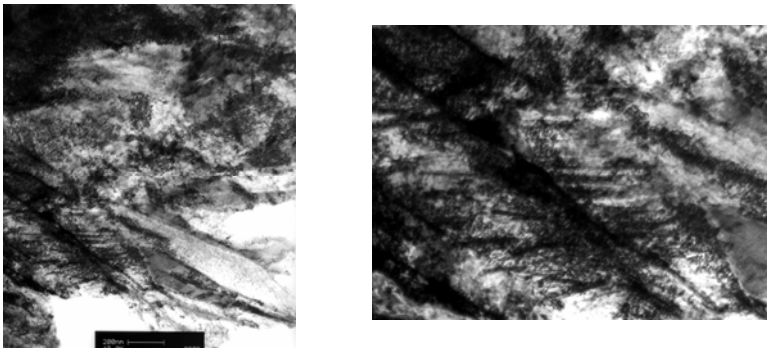

(a) **(b)**

Figure 5.16: (a) and (b) Thin foil dark field images of the circumference of the deformed region showing twinned martensite with dislocation pile-ups at twin interfaces in steel Q. Label mark 200 nm.

At 25mm away from the incidence direction the morphology was a twinned martensite with a large number of dislocations piled up at the twin interfaces. It appears that the twin interfaces are acting as dislocation barriers. This area has a higher Vickers micro-hardness than the centre of the impact area and also higher than the plate before the ballistic test.

The plate of steel R containing 2% retained austenite consisted of twinned martensite as well. At 2% the retained austenite is not easily observable in the dark field thin foil transmission electron microscopy images.

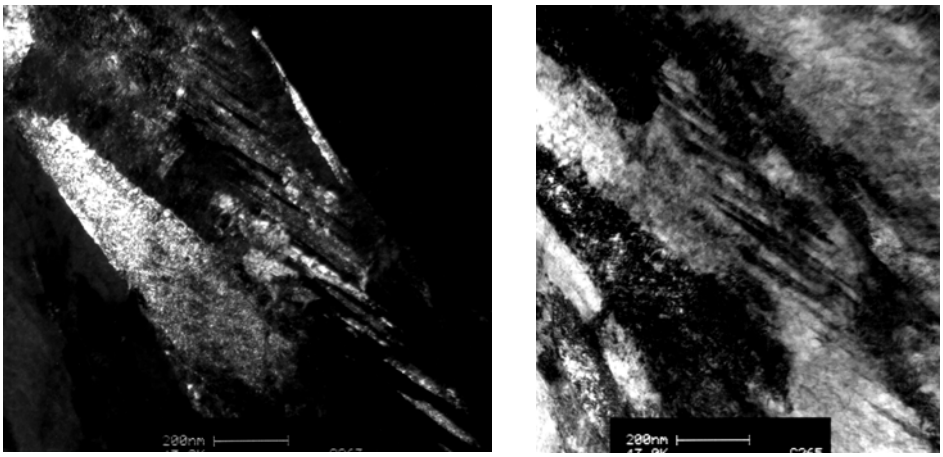

(a) **(b)**

Figure 5.17: (a) Thin foil dark field image and (b) corresponding bright field image of steel R before the ballistic test.

The bright field and dark field images of the centre of the impact area revealed untwinned martensite and the massive formation of fine carbides within the martensite plates and on the plate inter-faces despite its 1.03%Si content which should delay such a transformation.

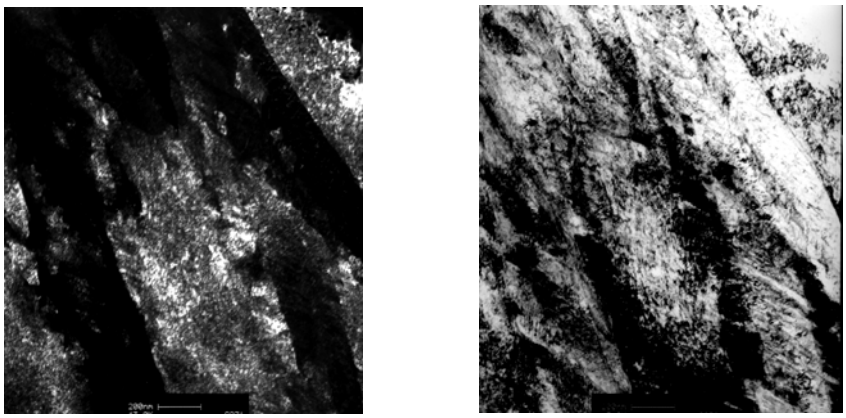

Figure 5.18: Thin foil transmission electron microscopy; (a) dark field and (b) the corresponding bright field image showing the disappearance of the twins and the formation of large aggregates of fine carbides throughout the martensite matrix at the centre of the ballistic impact area on the plate of steel R. Label mark 200 nm.

This formation of carbides may explain the decrease in the micro-hardness observed upon ballistic impact along the iso-depth line at one mm in Figure 5.12(c).

The plate of steel W contains 6% volume fraction of retained austenite and the nodules of retained austenite are located on the plate interfaces.

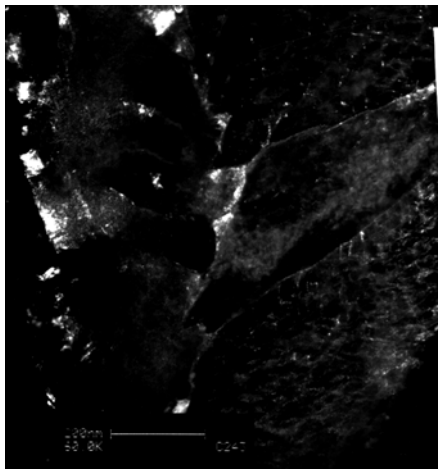

Figure 5.19: Dark field image thin foil transmission electron microscopy of steel W (0.98wt% Si) before the ballistic test. Label mark 200 nm.

Fine carbide particles have precipitated throughout the martensite plates upon tempering at 250°C for 15 minutes before the ballistic test.

Figure 5.20: Thin foil TEM bright field image showing the precipitation of fine carbides in the matrix before the ballistic test of steel W tempered at 250°C for 15 minutes. Label mark 200 nm.

The plate of steel T (the failed one) had the lowest volume fraction of retained austenite of about 0.6%, which is almost equal to the absolute error of detection by the X-ray diffraction equipment used. However, the thin foil transmission electron microscopy revealed elongated films of retained austenite along the lath interfaces. The measured martensite start temperature

of steel T was 184°C, which is comparable to those of the other seven steels successfully tested in this second series of ballistic testing. Nevertheless, it is still the highest M_s temperature in this series of steels. The morphology of the martensite before the ballistic testing was coarse laths with coarse cementite.
The cementite may have formed due to auto-tempering during the quenching and then coarsened upon tempering at 180°C. The low Silicon content of 0.4%Si was apparently not enough in this case to delay the formation of coarser cementite. The carbide particles around the perforation hole have coarsened further upon ballistic impact.

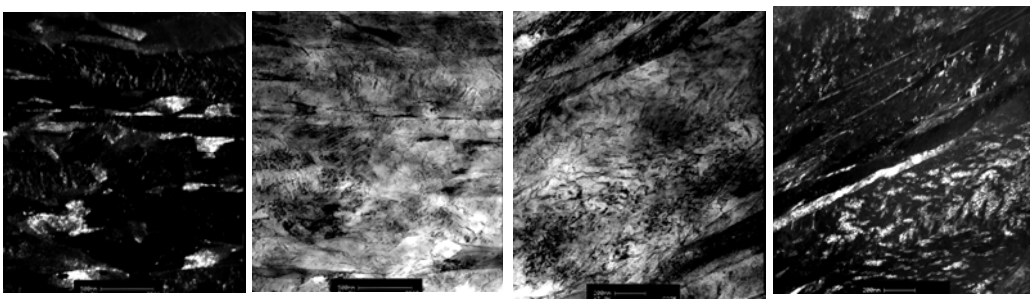

(a) (b) (c) (d)

Figure 5.21: Thin foil transmission electron microscopy of steel T; (a) and (b) dark field and corresponding bright field images before the ballistic test and (c) bright field image and (d) corresponding dark field image after the ballistic test, showing the coarsened carbide particles and the films of retained austenite. Label mark 500 nm.

5.5. General observation

The microstructure of the armour steel has a definite effect on its ballistic performance for plates with a thickness smaller than 6 mm and it is clear that there is a direct relationship between the microstructure and the ballistic performance of martensitic steel armour plates. The ballistic parameter BP, which takes into account the thickness of the plate and the volume fraction of retained austenite contained in the martensitic steel, may be used for predicting the ballistic performance and the following conclusions can be made at this stage.

(i) High ballistic performance may be achieved by combining twinned martensite with retained austenite in the same microstructure;
(ii) Coarse carbide particles are detrimental to the ballistic performance of the armour steels;
(iii) Stress-induced transformations occur inside the shock-affected region upon ballistic impact; and
(iv) The microstructure at the centre of the impact region does not contain any of the initial twins after impact.

The de-twinning process may be explained as follows: Part of the kinetic energy of the fired round is transformed into heat by entropy trapping, which raises the temperature high enough for the twinned martensite to recrystallise and re-austenitise. The new austenite is then quenched by the surrounding material and transforms into new untwinned martensite. This means that there is no memory effect present between the initial state with twinned martensite and the final state without twins. This transformation extends to a large volume around the impact region depending on the amount of retained austenite present in the plate. The kinetic energy of the fired round is then used to:

- heat up the surrounding material and induce the phase transformations; and
- mechanically deform the affected region.

The third part of the energy is transferred to the plate's support structure.

The phase changes during the ballistic impact should be considered in predicting the ballistic performance of a martensitic steel, as the fraction of the kinetic energy consumed by the phase transformation may be very important by resulting in a reduction of the effective energy available for the perforation stage.

The susceptibility of the retained austenite to stress-induced transformation appears to depend on its shape and location within the martensite. The nodular austenite, found when the volume fraction is higher than 2%, gave a stronger TRIP effect than the inter-lath films. This may be due to differences in the mechanical stability upon high strain rate impact of the two types of retained austenite.

Thin foil TEM of the experimental armour steels considered in this study revealed a change of the morphology of the retained austenite from film to nodular when its volume fraction increases. The ballistic performance of the experimental martensitic armour steels also increased as the volume fraction of retained austenite increased in the range from 1% to 6% although an upper limit has not been found within this range.

At too high volume fraction of retained austenite, adverse effects may occur following an excessive softening of the armour plates and the resistance to ballistic perforation. Further studies are needed on a possible upper limit of retained austenite content and to find an explanation on the mechanism by which retained austenite is transformed under impact, or whether a stress-induced or a strain-induced transformation occurs. Furthermore, investigations as to the location, the shape of the retained austenite and their mechanical and thermal susceptibilities will be useful in predicting and simulating the ballistic performance of martensitic armour steels containing some volume fraction of retained austenite.